Neuron
Article

Interplay of Cell-Autonomous and Nonautonomous Mechanisms Tailors Synaptic Connectivity of Converging Axons In Vivo

Haruhisa Okawa,[1] Luca Della Santina,[1] Gregory W. Schwartz,[2,3] Fred Rieke,[2,3] and Rachel O.L. Wong[1,*]
[1]Department of Biological Structure, University of Washington, Seattle, WA 98195-7420, USA
[2]Department of Physiology and Biophysics, University of Washington, Seattle, WA 98195-7290, USA
[3]Howard Hughes Medical Institute, Seattle, WA 98195, USA
*Correspondence: wongr2@uw.edu
http://dx.doi.org/10.1016/j.neuron.2014.02.016

SUMMARY

Neurons receive input from diverse afferents but form stereotypic connections with each axon type to execute their precise functions. Developmental mechanisms that specify the connectivity of individual axons across populations of converging afferents are not well-understood. Here, we untangled the contributions of activity-dependent and independent interactions that regulate the connectivity of afferents providing major and minor input onto a neuron. Individual transmission-deficient retinal bipolar cells (BCs) reduced synapses with retinal ganglion cells (RGCs), but active BCs of the same type sharing the dendrite surprisingly did not compensate for this loss. Genetic ablation of some BC neighbors resulted in increased synaptogenesis by the remaining axons in a transmission-independent manner. Presence, but not transmission, of the major BC input also dissuades wiring with the minor input and with synaptically compatible but functionally mismatched afferents. Cell-autonomous, activity-dependent and nonautonomous, activity-independent mechanisms thus together tailor connectivity of individual axons among converging inner retinal afferents.

INTRODUCTION

To generate their proper output, neurons must connect with appropriate presynaptic cell types as well as establish a stereotypic number of synapses with each input type. For example, each Purkinje cell in the cerebellum forms about 500 synapses with a single climbing fiber but makes more than 100,000 synapses with the population of parallel fibers, each parallel fiber contributing only a few synapses (Palay and Chan-Palay, 1974; Napper and Harvey, 1988). Consequently, activation of individual parallel fibers causes weak or no detectable responses in Purkinje cells (Isope and Barbour, 2002) whereas responses from the climbing fiber input are robust (Wadiche and Jahr, 2001). To understand how such stereotyped connectivity patterns are attained, it is necessary to elucidate the developmental processes that control the matching of synaptic partners, the relative convergence of distinct presynaptic cell types, and the number of connections formed by an individual axon onto a given postsynaptic cell. Indeed, many developmental mechanisms that navigate axons and dendrites toward their synaptic partners have been identified (Sanes and Yamagata, 2009; Shen and Scheiffele, 2010; Williams et al., 2010). We also have gained knowledge about the mechanisms that subsequently dictate the connectivity of the various afferent types, particularly with respect to their specific subcellular locations on the dendritic arbor (Cramer et al., 2004; Kerschensteiner et al., 2009; Hashimoto et al., 2009b; Phillips et al., 2011; DeNardo et al., 2012; Ding et al., 2012). However, what remain largely unknown are the relative roles of axon-axon and axon-dendrite interactions that establish the stereotypic connectivity patterns of each afferent type converging onto a common target cell. In the current study, we utilized a well-characterized circuit in the retina to uncover the precise roles of cell-autonomous and non-cell-autonomous interactions that shape synapse numbers at the level of individual axons within two distinct populations of converging afferents.

Retinal ganglion cells (RGCs) receive input from many types of glutamatergic bipolar cells (BCs) (Masland, 2012). Their compact circuitry readily facilitates mapping of the synapses between these cell types (Morgan et al., 2011; Schwartz et al., 2012). BCs are classified into two major functional types, ON and OFF BCs, that are depolarized and hyperpolarized by increased illumination, respectively. ON and OFF BCs each comprise several subtypes that are distinguished by their characteristic morphologies and axonal stratifications within separate ON and OFF synaptic laminae in the inner plexiform layer (IPL) (Wässle et al., 2009; Helmstaedter et al., 2013). RGCs are also diverse, but each major functional type stratifies its dendrites at a specific depth of the IPL in order to contact functionally matched BC axons. Like other circuits in the brain, RGCs exhibit stereotypic wiring patterns with presynaptic BCs. We previously found that one RGC type, the $A_{ON\text{-}S}$ RGC (or G10) that responds to light onset with sustained spiking, makes about 70% of its synapses with type 6 (T6) ON BCs (major input) and consistently makes fewer synapses with type 7 (T7) ON BCs (minor input) (Schwartz et al., 2012). Blockade of neurotransmission from all ON BCs selectively regulates T6, but not T7, connectivity with $A_{ON\text{-}S}$ RGCs (Kerschensteiner et al., 2009; Morgan et al.,

2011). What remains unclear is whether neurotransmission only regulates connectivity of specific types of BCs or whether there are as yet unmasked synaptogenic "rules" that define the stereotypic wiring patterns of each input type in the circuit. Here, we asked whether, among converging inputs, transmission sets the number of synapses made by axons at the population level (i.e., T6 versus T7) or whether it dictates connectivity at the level of individual axons of the same type. As such, we performed two in vivo manipulations—(1) varying the density of transmitting versus nontransmitting BCs within the dendritic field of the RGCs and (2) partially ablating populations of BCs genetically. The first manipulation allowed us to specifically ask whether presynaptic transmission acts locally or globally across the dendritic arbor to regulate synaptic connectivity, and the second manipulation enabled an investigation of potential wiring limits set by axon-axon interactions that may be independent of transmission.

Surprisingly, we found that activity of an individual BC influences its own connectivity without affecting the connectivity of neighboring BCs, of the same or different type, that share the dendrite. This lack of "competition" contrasts markedly with previous studies showing that an imbalance of transmission among converging axons leads to synaptic competition (Antonini and Stryker, 1993; Buffelli et al., 2003; Yu et al., 2004; Hua et al., 2005; Hashimoto et al., 2009a; Ben Fredj et al., 2010; Yasuda et al., 2011). In addition, our BC ablation experiments revealed a mechanism that relies on the presence of, but not on transmission from, the dominant T6 BC input. T6 BCs limit synaptogenesis with the minor but appropriate T7 input, as well as restrict wiring with inappropriate OFF BC axons. Together, our findings delineate distinct and nontraditional roles of activity-dependent and independent mechanisms that operate in concert to establish the stereotypic wiring patterns of a set of converging sensory axons.

RESULTS

Neurotransmission Locally Regulates Synapse Size and Density on $A_{ON\text{-}S}$ RGC Dendrites

We previously generated a transgenic mouse line in which a promoter fragment of metabotropic glutamate receptor 6 (*Grm6*) drives expression of the light chain of tetanus toxin (TeNT) and yellow fluorescent protein (YFP). Activity of the exogenous *Grm6* promoter is limited to ON-BCs in the retina, but its activation pattern among ON-BCs varies across founders. Our previous study specifically identified a founder that expresses TeNT/YFP in all ON-BCs (*Grm6-TeNT* ^{pan}; Figures S1A and S1D available online) (Kerschensteiner et al., 2009). We found that suppressing neurotransmitter release from all ON-BCs does not perturb axonal morphology of BCs or dendritic organization of $A_{ON\text{-}S}$ RGCs. However, the average density of synapses made between these synaptic partners (Figure 1A) is reduced (Kerschensteiner et al., 2009; Morgan et al., 2011).

To determine whether ON-BC transmission regulates synapse density globally across the entire dendritic arbor or locally at sites of transmission, we screened other *Grm6-TeNT* potential founders and obtained a line in which patches of ON-BCs express YFP and TeNT (*TeNT* ^{patchy}) (Figures 1B, S1B, and S1E). This "patchy" expression creates an arrangement whereby the arbor of a RGC comprises segments of dendrites that receive either active or inactive inputs. We confirmed that, in *TeNT* ^{patchy} mice, TeNT-expressing BCs lack the uncleaved form of vesicle-associated membrane protein 2 (VAMP2), a protein necessary for vesicle fusion (Figure 1C). The patchy TeNT expression pattern created an imbalance in neurotransmission among neighboring ON-BCs converging onto the dendritic arbor of individual $A_{ON\text{-}S}$ RGCs. To directly compare the connectivity of YFP/TeNT$^+$ and YFP/TeNT$^-$ axons on the same RGC, we biolistically cotransfected RGCs with plasmids driving expression of a fluorescent protein, tdTomato, and postsynaptic density protein 95 fused to cyan fluorescent protein (PSD95-CFP) (Figure 1D). We then mapped PSD95-CFP puncta apposed to YFP/TeNT$^+$ BC terminals (inactive synapses) and those not apposed to YFP-labeled terminals (active synapses) across the dendritic arbor of individual $A_{ON\text{-}S}$ RGCs (Figure 1E). Dendritic segments comprising predominantly active synapses (active segments) or inactive synapses (inactive segments) were thus identified (Figure 1F; see Experimental Procedures for definition of "active" and "inactive" segments).

We noticed that PSD95-CFP clusters were significantly larger at inactive synapses (Figures 1G–1I; active: 0.21 ± 0.01 μm^3; inactive: 0.28 ± 0.01 μm^3, mean ± SEM, n = 11; $p < 0.001$), resembling a homeostatic response previously observed in some circuits (Turrigiano and Nelson, 2004; Davis, 2006), but not others (Burrone et al., 2002; Harms et al., 2005). This morphological change was localized to inactive synapses, as PSD95-CFP clusters at nearby active synapses, even along the same dendritic branch, appeared unaffected. Because the density of TeNT$^+$ BCs varied across retinas and within each retina, the proportion of the total synapses on a given RGC that were inactive was variable. However, despite this variability, PSD95-CFP puncta density was always lower along inactive segments compared to active segments in individual RGCs (Figure 1J). The lack of a systematic correlation between the average synapse density of the active or inactive segments and the fraction of total synapses that were inactive implied that there was no compensatory increase in synapse density either locally or globally. RGCs with small or large fractions of synapses that were inactive all showed densities of active synapses similar to that of wild-type cells (Figure 1J). Thus, neurotransmission regulates synapse density locally, only reducing the number of synapses on dendrites contacted by inactive axonal terminals. Remarkably, differences in PSD95-CFP puncta density along a dendrite occurred within 10 μm from the boundary between TeNT$^+$ and TeNT$^-$ patches (Figure 1K). This short distance is roughly the diameter of the axonal arbor of a T6 BC, thus raising the possibility that synaptic connectivity of a RGC can be regulated by neurotransmission at the level of contact with individual axons without changes in connectivity with other afferents.

Neurotransmission Regulates the Connectivity of Individual T6 BC Axons Cell Autonomously

To test the hypothesis that transmission regulates connectivity of individual axons independently, we obtained another mouse line, *Grm6-TeNT* ^{sparse}, in which isolated ON-BCs, including T6 BCs, express YFP and TeNT (Figures 2A, S1C, and S1F). As in other

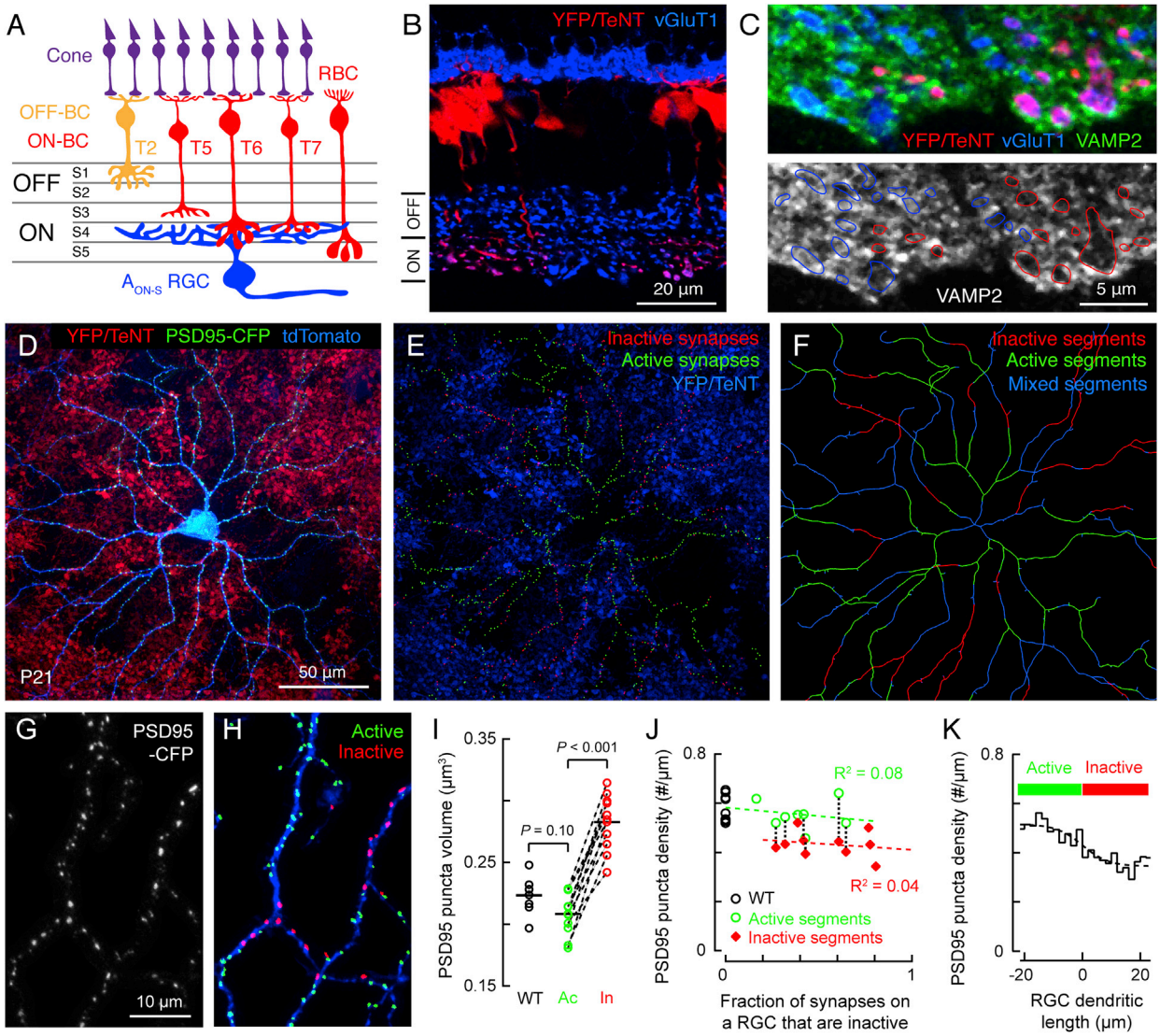

Figure 1. Neurotransmission Locally Regulates Postsynaptic Size and Densities on RGC Dendrites

(A) Schematic of the axonal stratification of the major bipolar cell (BC) types and the RGC examined in this study. RBC, rod bipolar cell. $A_{ON\text{-}S}$ RGC dendrites stratify in sublamina 4 (S4), where they contact the axon terminals of T6 and T7 ON-BCs.

(B) Vibratome section of a postnatal day 21 (P21) *Grm6-TeNT patchy* retina showing columns of YFP/TeNT-expressing ON-BCs. ON- and OFF-BC axon terminals are immunopositive for vesicular glutamate transporter 1 (vGluT1).

(C) Magnified view of BC axon terminals in adjacent YFP/TeNT$^+$ and YFP/TeNT$^-$ regions. BC axon terminals were visualized by vGluT1 immunostaining. VAMP2 intensity appears reduced in YFP$^+$/vGluT1$^+$ boutons (e.g., red outlines), compared to YFP$^-$/vGluT1$^+$ (e.g., blue outlines) boutons.

(D) Whole-mount view of a $A_{ON\text{-}S}$ RGC biolistically labeled by cytosolic tdTomato and PSD95-CFP expression in *Grm6-TeNT patchy* retina at P21.

(E) Distribution of PSD95-CFP puncta that were apposed (red; "inactive synapses") or not apposed (green; "active synapses") to TeNT$^+$ BC axons.

(F) Dendritic segments dominated (>85% of synapses) by inactive synapses are shown in red ("inactive segments"), those dominated by active synapses in green ("active segments"), and all remaining segments in blue ("mixed segments") for the cell in (D). See Experimental Procedures for details.

(G) Maximum intensity projections of PSD95-CFP puncta in active and inactive regions.

(H) Two-dimensional representation of puncta volumes in (G). See Experimental Procedures.

(I) Average PSD95-CFP puncta volume for $A_{ON\text{-}S}$ RGCs in wild-type (WT) and *Grm6-TeNT patchy* retinas at P21–P23. Active (Ac) and inactive (In) synapses were averaged separately. Dotted lines connect data from the same cell. Horizontal bars indicate means of the distributions.

(J) PSD95-CFP puncta densities averaged across all active or inactive segments of each RGC plotted against the fraction of the total number of synapses that were inactive for the cell (WT; wild-type had no inactive synapses). Vertical dotted lines connect data points from the same RGC. Linear regression fits indicate no significant correlation between average puncta density and the proportion of synapses that were inactive (active segments: $R^2 = 0.08$, $p = 0.29$; inactive segments: $R^2 = 0.04$, $p = 0.57$).

(K) Average PSD95-CFP puncta density along dendritic lengths with sharp transitions (see Experimental Procedures) between active and inactive patches (84 dendritic segments from 11 $A_{ON\text{-}S}$ RGCs).

See also Figure S1.

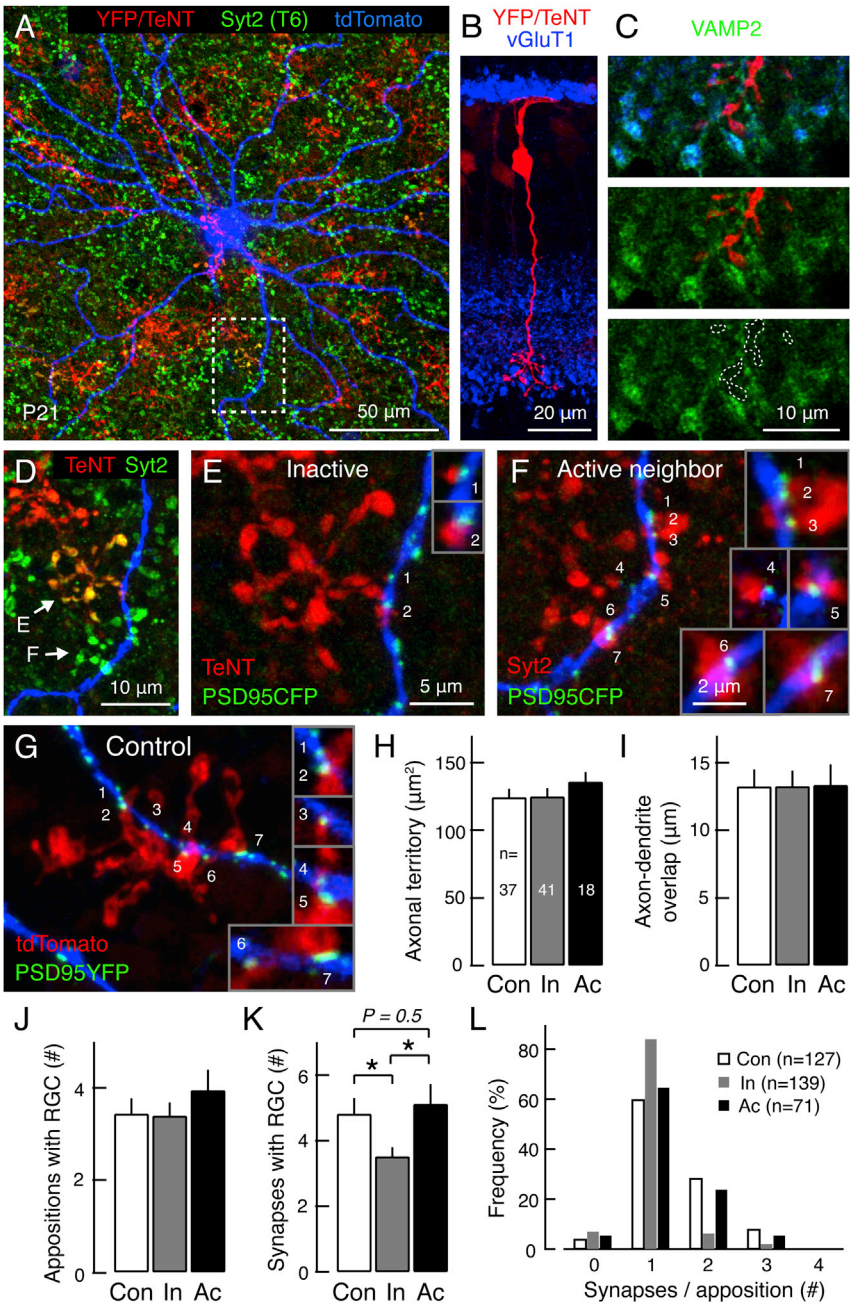

Figure 2. Activity-Regulated Connectivity of Individual Axons Occurs without Synaptic Competition

(A) A representative $A_{ON\text{-}S}$ RGC biolistically labeled by tdTomato in *Grm6-TeNT* ^{sparse} retina at P21. T6 BC axon terminals are immunopositive for synaptotagmin-2 (Syt2).

(B) An isolated YFP/TeNT^{+} T6 BC in *Grm6-TeNT* ^{sparse} retina.

(C) Magnified views showing that VAMP2 expression was selectively reduced in the YFP/TeNT^{+} T6 BC axon terminal (e.g., outlines; see Movie S1 for through series).

(D) Magnified view of the boxed region in (A) showing a pair of TeNT^{+} (inactive) and TeNT^{-} (active) T6 BC neighbors contacting the same dendrite of an $A_{ON\text{-}S}$ RGC.

(E and F) Synapses made by the inactive T6 BC and the active neighbor. The active axon shows characteristic multiple PSD95-CFP puncta (1–3 and 6 and 7) apposed to a single bouton (see control; G). Insets show enlarged views of synapses in single confocal planes.

(G) A representative control T6 BC in the *Grm6-tdTomato* mouse retina (Kerschensteiner et al., 2009; Morgan et al., 2011) and its synapses with an $A_{ON\text{-}S}$ RGC. Images of the axons and insets in (E–G) are at the same magnification.

(H–K) Quantification of axonal parameters and connectivity of P21 control (Con, white), inactive (In, gray), and neighboring active (Ac, black) T6 BCs. n, number of T6 BC-$A_{ON\text{-}S}$ RGC pairs. Bar graphs show the mean + SEM. p value: *p < 0.05.

(L) Distribution of the number of PSD95-CFP puncta associated with each BC apposition for control, inactive, and neighboring active T6 BCs. n, number of appositions analyzed.

See also Figure S1.

Grm6-TeNT lines, we confirmed that the isolated TeNT-expressing T6 BCs visualized by coexpression of YFP had greatly reduced VAMP2 expression compared to surrounding YFP^{-} BCs (Figures 2B and 2C; Movie S1). Immunolabeling T6 BC population using anti-synaptotagmin-2 (Syt2) allowed for a direct comparison of the number of synapses made by individual active and inactive T6 axons along a dendritic branch (Figure 2D). Figures 2E–2G provide examples of the synaptic contacts of an active and an inactive T6 BC in the *TeNT* ^{sparse} retina and in a control axon labeled sparsely in the *Grm6-tdTomato* mouse (Kerschensteiner et al., 2009; Morgan et al., 2011).

In the *TeNT* ^{sparse} line, the axon terminal size of inactive T6 BCs was similar to that of neighboring active T6 BCs and to control T6 BCs (Figure 2H). Our result contrasts with findings from other systems in which activity differences between neighboring axons cause a differential change in axonal territories (Buffelli et al., 2003; Yu et al., 2004; Hua et al., 2005; Hashimoto et al., 2009a; Ben Fredj et al., 2010; Yasuda et al., 2011). The average spatial overlap of $A_{ON\text{-}S}$ RGC dendrites and T6 axonal terminals was not significantly different across conditions, suggesting that $A_{ON\text{-}S}$ dendrites did not avoid inactive T6 BCs or vice versa (Figure 2I). The number of appositions (presumed sites of axon-dendrite contact) made by each inactive axon with a $A_{ON\text{-}S}$ dendrite was unchanged (Figure 2J), but inactive T6 BCs made fewer synapses with $A_{ON\text{-}S}$ RGCs compared to active T6 neighbors and to control T6 BCs (Figure 2K). This reduction was due to a failure of the inactive T6 axon to consistently establish multisynaptic boutons, characterized by several release sites (ribbons), each apposed to a separate PSD95 cluster (Kerschensteiner et al.,

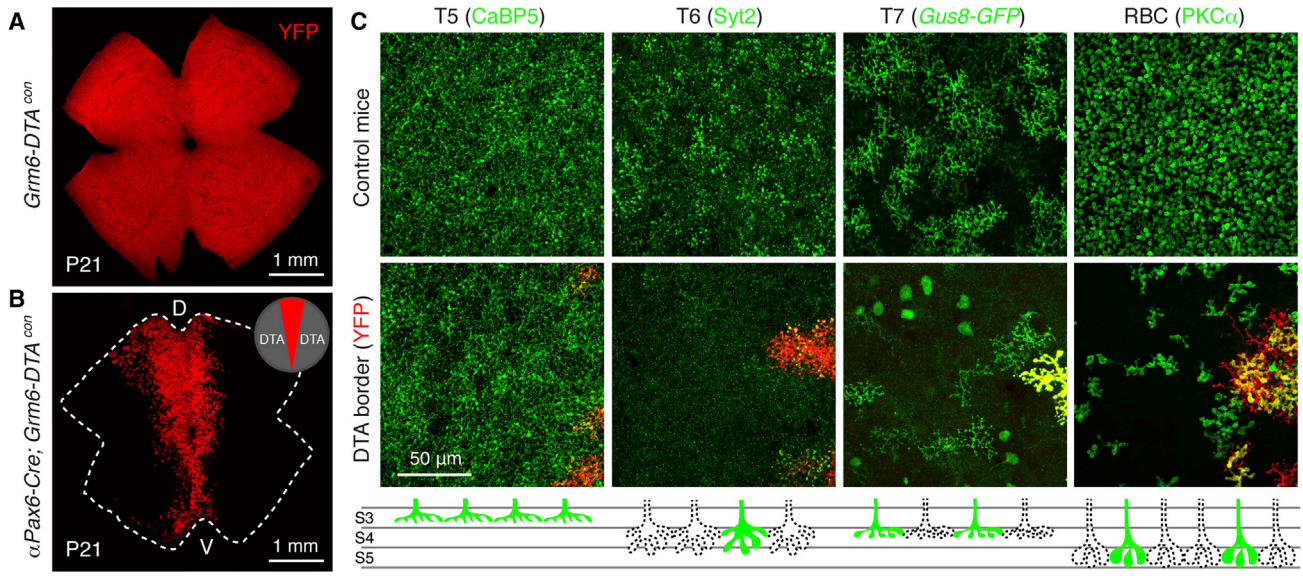

Figure 3. Ablation Pattern of ON Bipolar Cells in *αPax6-Cre*; *Grm6-DTA*^{con} Mice

(A) YFP expression in *Grm6-DTA*^{con} mouse retina before Cre-recombination.

(B) Whole-mount retina from a *αPax6-Cre*; *Grm6-DTA*^{con} mouse showing a dorsoventral wedge of YFP^{+} cells flanked by regions where ON BCs are ablated (DTA-expressing). D, dorsal; V, ventral.

(C) Visualization of remaining axon terminals for each ON BC type at the border of DTA- and non-DTA-expressing regions. Immunostaining for calcium-binding protein 5 (CaBP5), Syt2, and protein kinase C alpha (PKCα) labels T5, T6, and RBC axon terminals, respectively. T7 BCs were identified by crossing *αPax6-Cre*; *Grm6-DTA*^{con} with *Gus8-GFP* mice, in which a large population of T7 BCs express GFP (Huang et al., 2003). Wild-type mice are used as control for T5, T6, and RBC labelings. Below the images are schematics illustrating axon types that are present (green) or ablated (dotted). In the DTA-expressing regions, virtually all T5 BCs are present, a large population of T6 BCs are ablated, and some T7 and RBCs are also ablated. The scale bar applies to all images.

2009; Morgan et al., 2011) (Figure 2L). As in the *TeNT* ^{patchy} line, PSD95-CFP puncta formed by *TeNT* ^{sparse} axons were significantly larger compared to that of active neighbors (inactive: 0.33 ± 0.02 µm^3, n = 28; active neighbor: 0.28 ± 0.01 µm^3, n = 18; $p < 0.05$). Neighboring active T6 BCs did not increase their axonal size or synaptic contact with the RGC (Figures 2H and 2K). Thus, activity regulates synapse number and organization of T6 contacts on a cell-by-cell basis. Collectively, our observations suggest that establishing the normal synapse number between individual T6 axons and $A_{ON\text{-}S}$ RGC dendrites relies on neurotransmission in a cell-autonomous manner and is not sculpted by activity-dependent competition among converging axons.

Neighboring BC Axons Limit T6 Axon Territories and Their Synaptic Connectivity

BCs of the same type form mosaics with minimal dendritic and axonal overlap, a phenomenon called "tiling" (Wässle et al., 2009). This structural arrangement ensures that there are no gaps in the sampling of an image. Axonal tiling raises the possibility that a second mechanism exists to regulate the connectivity of individual BC axons and that this mechanism involves interactions between converging presynaptic neighbors. We thus genetically ablated some BCs by generating conditional transgenic mice (*Grm6-DTA*^{con}) in which ON-BCs express the attenuated form of diphtheria toxin (DTA) upon Cre recombination in place of YFP (Figure 3A). These mice were bred with a retina-specific Cre driver line, *αPax6-Cre* mice, to restrict the ablation to the retina (Marquardt et al., 2001). *αPax6* expression is scarce along the dorsoventral wedge of the retina, creating regions with and without the full complement of BCs (Figure 3B). Due to early activation of *αPax6* and *Grm6*, ON-BCs are likely ablated by the end of the first postnatal week (P7), when these neurons begin elaborating axonal branches to contact RGCs (Morgan et al., 2006). To determine which ON-BC types were ablated, we distinguished T5, T6, T7, and rod bipolar cells (RBCs) using a combination of immunohistochemical markers and transgenic mice expressing GFP. As shown in Figure 2A, T6, but not T7, BCs are labeled by the anti-Syt2 antibody. T7 BCs, but not T6 BCs, express GFP in *Gus8-GFP* mice (Huang et al., 2003). We found that, within the DTA-expressing regions, T6 BCs were largely missing; some T7 and RBCs were also ablated, whereas T5 BCs were unaffected (Figure 3C).

We biolistically labeled $A_{ON\text{-}S}$ RGCs in the DTA region and analyzed their connectivity with surviving BCs (Figure 4A). We further performed SMI-32 immunolabeling for neurofilament H, known to label this RGC type (Bleckert et al., 2014), as a means of identifying $A_{ON\text{-}S}$ RGCs in the DTA region (Figure S2). As shown in Figure 3C, T6 BCs are largely absent in the DTA-expressing regions. Variability in the intensity of YFP expression and Syt2 labeling among T6 BCs in *Grm6-DTA*^{con} retina allowed us to identify and segment individual T6 BC axons (Figure 4B). Surviving T6 BC axons maintained tiling with remaining neighbors (Figure 4C) and formed synapses (Figure 4D). The axon terminals of surviving BCs became larger (Figure 4E), but their expansion did not fully cover the cell-ablated regions (Figure 4C).

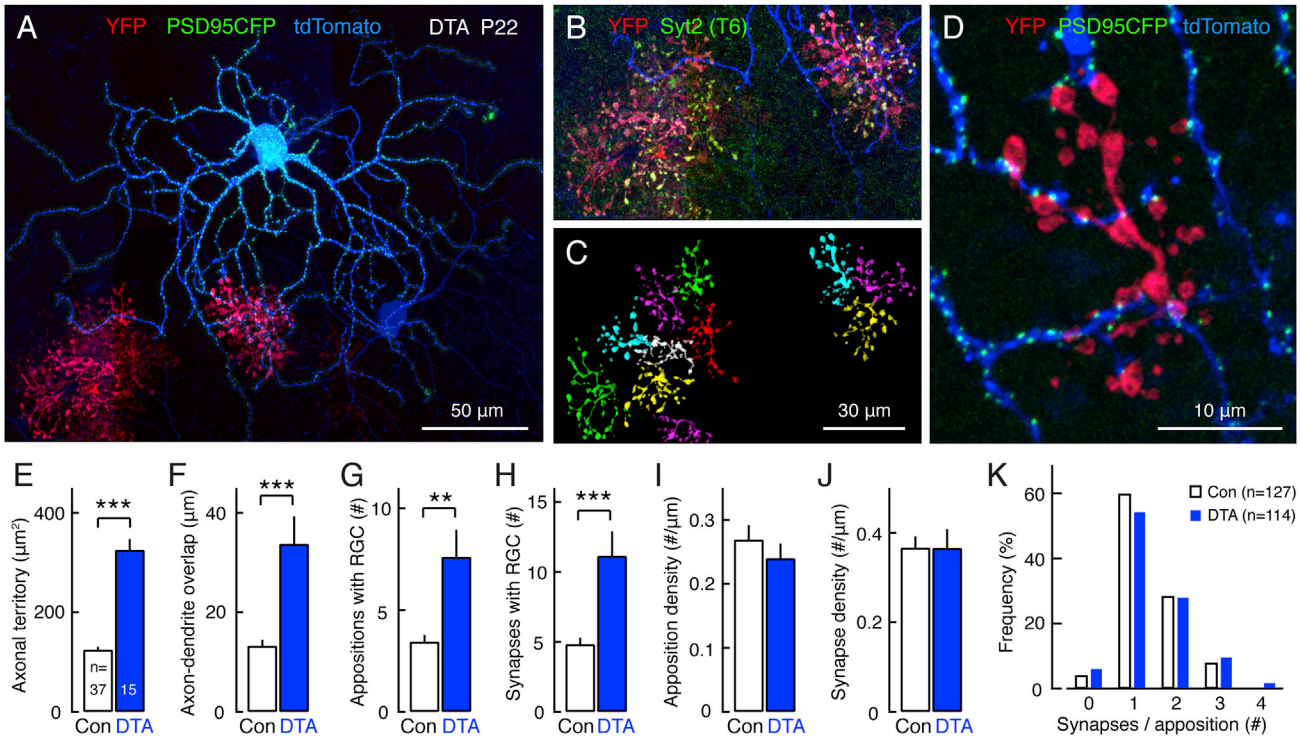

Figure 4. Bipolar Cell Neighbors Constrain Synaptic Connectivity by Limiting Axonal Territories

(A) An $A_{ON\text{-}S}$ RGC at the border between DTA- and non-DTA-expressing regions.

(B) Syt2 labeling identifies patches of YFP^{+} BCs as T6 BCs.

(C) Axon terminals of each T6 BC within the patches in (B) were digitally segmented and pseudocolored.

(D) Connectivity of one of the remaining T6 BCs with the $A_{ON\text{-}S}$ RGC.

(E–J) Quantitative comparison of P21–P23 control (Con) and surviving T6 BCs (DTA). Apposition and synapse densities (I and J) were obtained by dividing the total counts (G and H) by the amount of axon-dendritic overlap (F). n, number of T6 BC-$A_{ON\text{-}S}$ RGC pairs. The bar graphs show mean + SEM. p values: $^{**}p < 0.01$, $^{***}p < 0.001$.

(K) Distributions of the number of PSD95-CFP puncta at each apposition for control and surviving T6 BCs. n, number of appositions.

See also Figure S2.

This axonal overgrowth led to greater overlap with $A_{ON\text{-}S}$ dendrites (Figure 4F) and more appositions and synapses with these RGCs (Figures 4G and 4H). Thus, in the physical absence of neighboring BCs, largely those of the same type, T6 BCs can increase synaptic connectivity by expanding their axonal territory. This expansion in axonal territory and the associated increase in synapse number are not dependent on T6 transmission because transmission-deficient T6 BCs have normal axonal size. Interestingly, the densities of appositions and synapses made between each surviving T6 axon and the $A_{ON\text{-}S}$ RGC were unchanged (Figures 4I and 4J). Also, the number of synapses per apposition was similar to that of control retina (Figure 4K). Thus, T6 axons maintain their characteristic synaptic arrangements, even when their axonal terminals and connectivity with $A_{ON\text{-}S}$ RGCs is increased.

T7 BCs Increase Synaptic Connectivity in the Absence of T6 BCs

We noticed that, even in the absence of their major input, the T6 BCs, $A_{ON\text{-}S}$ RGCs in DTA regions unexpectedly maintained a density of PSD95-CFP puncta comparable to that of wild-type $A_{ON\text{-}S}$ RGCs (Figures 4A and 7E). To test whether these PSD95-CFP puncta have presynaptic appositions with remaining non-T6 BCs, we crossed *αPax6-Cre*; *Grm6-DTA^{con}* mice with *Grm6-GFP* mice in which all the ON-BCs express GFP (Morgan et al., 2006). YFP was distinguished from GFP, enabling the correct identification of DTA regions (Figures 5A–5C). Approximately 50% of the PSD95-CFP puncta were apposed to ON-BC terminals in DTA regions, whereas in control retinas, ~90% are apposed to ON-BCs (Figures 5D–5F). In addition, a large proportion of PSD95-CFP puncta colocalized with CtBP2, a presynaptic ribbon marker, in DTA regions (Figures 5G–5I). Because T6 BC input accounts for ~70% of PSD95 puncta on $A_{ON\text{-}S}$ RGC dendrites in wild-type retinas (Schwartz et al., 2012), this result suggests that other BC types increased synaptic contact with the $A_{ON\text{-}S}$ RGC.

To test whether surviving T7 BCs in regions devoid of T6 BCs compensate for the loss of synapses normally formed by T6 BCs, we crossed *αPax6-Cre*; *Grm6-DTA^{con}* mice with *Gus8-GFP* mice in which a large population of T7 BCs are labeled by GFP (Huang et al., 2003). We quantified the connectivity of surviving T7 BCs with $A_{ON\text{-}S}$ RGCs in DTA-expressing regions where all the T6 BCs as well as some T7 BCs were ablated (Figures 6A and 6B). We compared these measurements with that of control T7 BCs visualized in the *Grm6-tdTomato* line (Kerschensteiner

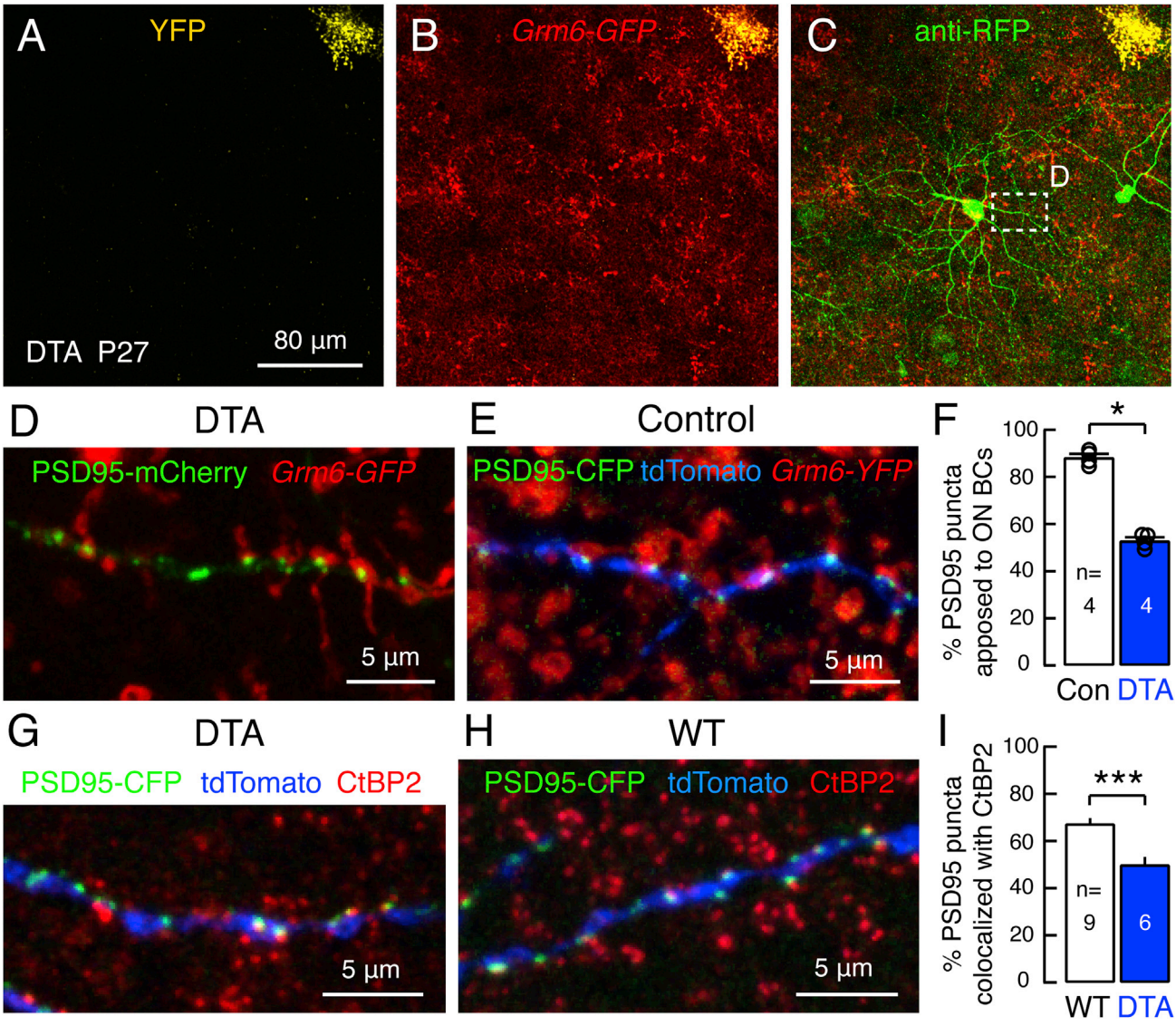

Figure 5. Non-T6 BCs Appear to Take Over Synaptic Sites of Ablated T6 BCs

(A and B) Top view of remaining ON-BC axon terminals in a DTA region visualized by crossing *αPax6-Cre*; *Grm6-DTA*^{con} mice with *Grm6-GFP* mice, in which all ON-BCs are labeled by GFP (Morgan et al., 2006). YFP was distinguished from GFP using laser excitations at 488 and 515 nm, which enabled identification of DTA (non-YFP) regions.

(C) An $A_{ON\text{-}S}$ RGC transfected with plasmid encoding PSD95-mCherry. Immunolabeling for mCherry with an antibody against red fluorescent proteins (RFPs) enhanced the PSD95-mCherry puncta but also labeled cytosolic PSD95-mCherry, which facilitated the search for transfected RGCs.

(D) Magnified view of the boxed region in (C). Many PSD95-mCherry puncta were apposed to surviving ON-BC axons.

(E) The appositions of PSD95 puncta with ON-BCs in control $A_{ON\text{-}S}$ RGCs were examined using *Grm6-YFP* mice (*Grm6-DTA*^{con} mice without crossing with *αPax6-Cre* mice).

(F) Percentage of PSD95 puncta apposed to ON-BCs for individual $A_{ON\text{-}S}$ RGCs in control (Con) mice and for contacts in the ON layer of DTA-expressing regions. Bar graph shows average + SEM. p value: *$p < 0.05$.

(G–I) Colocalization of PSD95 puncta and presynaptic ribbons (CtBP2). The colocalization rate of contacts on the dendrites within the ON sublamina of cells in the DTA region was lower than that of WT. n, the number of $A_{ON\text{-}S}$ RGCs. The bar graph shows average + SEM. p value: ***$p < 0.001$.

et al., 2009; Morgan et al., 2011) (Figure 6C). We found that surviving T7 BCs expanded their axon terminals (Figure 6D), most likely resulting from the ablation of some T7 BC neighbors. The enlarged axon terminals led to an increased overlap with $A_{ON\text{-}S}$ RGC dendrites (Figure 6E) and an increased number of synapses with the RGC (Figure 6F). These changes resemble those of T6 BCs in the DTA regions but with an important difference. Unlike T6 BCs, synapse density on $A_{ON\text{-}S}$ RGC dendrites associated with T7 BC input was much higher in the DTA regions compared to that in control retina (Figure 6G) and even approached the synapse density of T6 BCs (Figure 6H). In addition, presynaptic ribbons were present at these synaptic sites (CtBP2-positive;

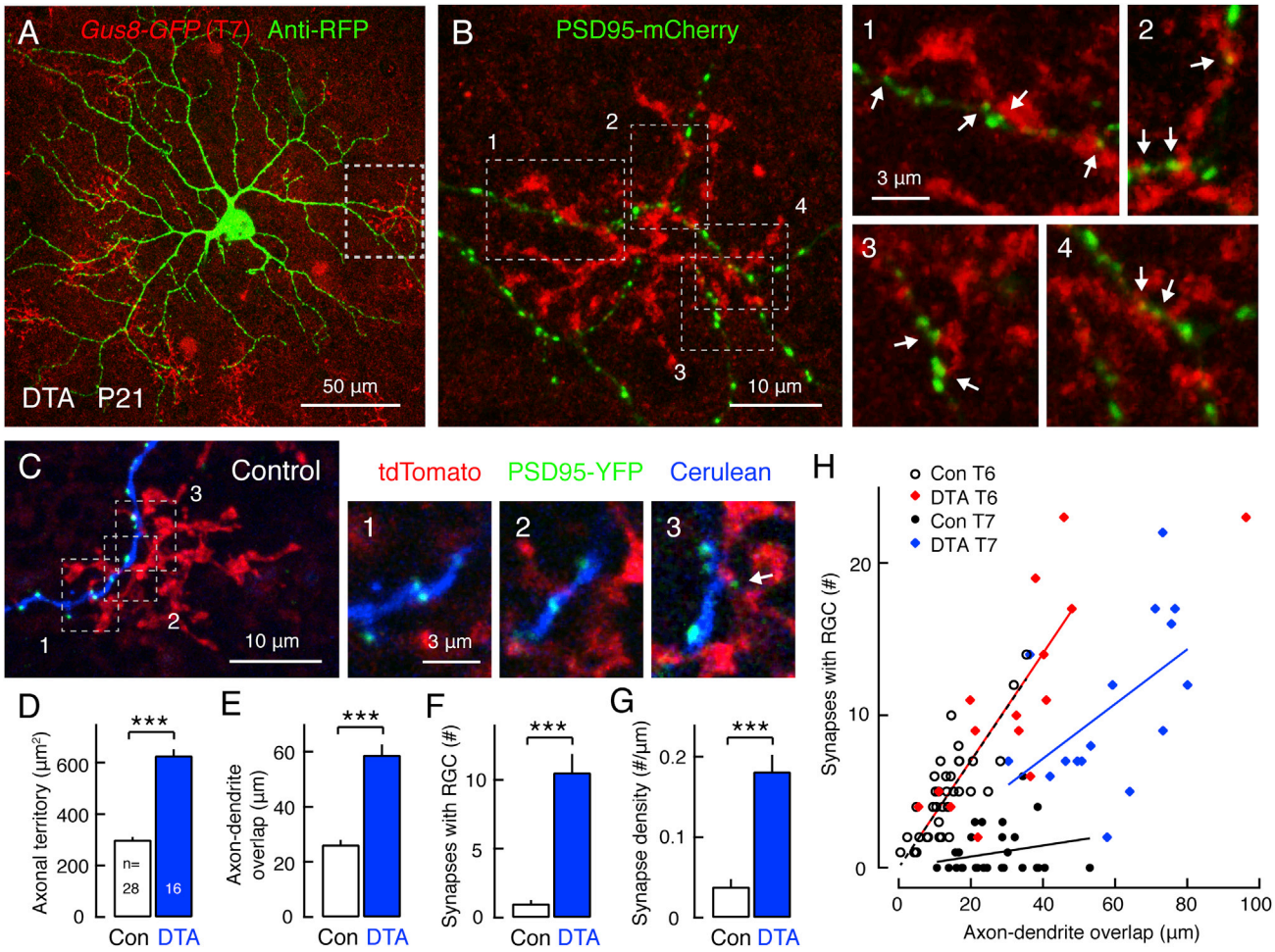

Figure 6. T7 Bipolar Cells Increase Connectivity with A_{ON-S} RGCs in the Absence of T6 Bipolar Cells

(A) Top view of remaining T7 BC axon terminals and an A_{ON-S} RGC visualized in a DTA region of a *αPax6-Cre*; *Grm6-DTA^{con}*; *Gus8-GFP* retina at P21. The RGC was biolistically transfected with PSD95-mCherry followed by immunostaining with anti-RFP to enhance both punctate and cytosolic mCherry.

(B) An isolated T7 BC boxed in (A). Higher magnifications of the synapses (arrows) in four regions are provided. Each image (1–4) is the maximum intensity projection of three consecutive confocal sections spanning ~1 µm in thickness. The scale bar applies to all four images (1–4).

(C) Contact between a control T7 BC and an A_{ON-S} RGC in a *Grm6-tdTomato* mouse. Only one synapse (arrow in image 3) was identified, typical of the connectivity between T7 BCs and this type of RGC (Morgan et al., 2011). The enlarged views are maximum intensity projections of three to six consecutive confocal sections spanning ~1.0–1.5 µm in thickness showing that other PSD95-mCherry puncta within the overlap of the axonal field and the dendrite were not apposed to the BC terminal. The scale bar (3 µm) applies to images 1–3.

(D–G) Quantitative measures for control (Con) T7 BCs and remaining T7 BCs in DTA regions. Bar graphs show mean + SEM. p values; ***$p < 0.001$.

(H) Synapse number plotted against the length of axon-dendrite overlap for each pair of a T6 or a T7 BC with an A_{ON-S} RGC. The slope of the line fit (control T6 BCs, dashed black; DTA T6 BCs, red; control T7 BCs, solid black; DTA T7 BCs, blue) indicates the density of synapses.

See also Figure S3.

144 of 168 synapses). If surviving T7 BCs took over only the synapses of ablated T7 neighbors, synapse density might have been unchanged as shown for T6 BCs. We suggest that the increased synapse density of surviving T7 BCs indicate that these cells also took over postsynaptic territory that was normally occupied by other (T6) BCs. If this takeover were triggered by the lack of T6 transmission, a similar scenario would have occurred in the dendritic segments contacted by TeNT-expressing T6 BCs. However, along the dendrite innervated by an inactive T6 axon, non-T6 synapses remained at densities similar to control (Figure S3), suggesting that increased T7 BC-A_{ON-S} RGC connectivity in the DTA regions is activity-independent. Our findings here underscore that, during normal development, BC axons within and across populations constrain the synaptic territory and connectivity of neighboring axons in an activity-independent manner.

A_{ON-S} RGCs Form Ectopic Synapses Selectively with T2 OFF BCs in the Absence of Major ON Inputs

Dendritic arbors of A_{ON-S} RGCs remain stratified in the ON sublamina, even when all their excitatory inputs are silenced in *Grm6-TeNT ^{pan}* mice (Kerschensteiner et al., 2009). In

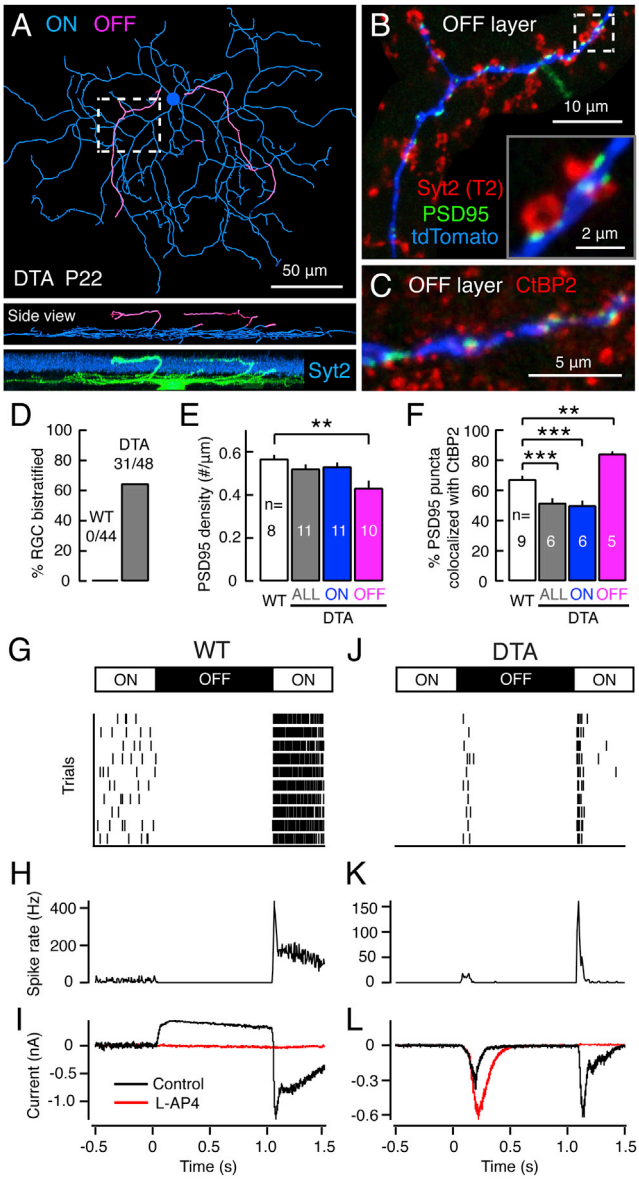

Figure 7. $A_{ON\text{-}S}$ RGCs Form Ectopic Functional Synapses with OFF-BCs in the Absence of Major ON Inputs

(A) Skeletonized dendrites of the $A_{ON\text{-}S}$ RGC in Figure 4A and their spatial distribution across the ON and OFF sublaminae.

(B) Magnified view of a dendritic branch in the OFF layer within the boxed region in (A). Syt2 is also expressed by T2 BCs. Shown here is the maximum intensity projection of an expanded volumetric digital mask of the dendrite and Syt2 fluorescent signals, allowing the OFF dendritic branch and its synapses with T2 BC axons to be more readily discerned. The inset is an enlargement of the boxed region.

(C) PSD95-CFP puncta along an ectopic OFF dendritic branch of a different $A_{ON\text{-}S}$ RGC showed good colocalization with presynaptic ribbons (anti-CtBP2) in BC axon terminals.

(D) Thirty-one of forty-eight $A_{ON\text{-}S}$ RGCs in the DTA-expressing regions had ectopic dendrites in the OFF sublamina, whereas dendrites of $A_{ON\text{-}S}$ RGCs in WT were always restricted to the ON sublamina.

(E) Average PSD95-CFP puncta densities of normally placed (ON), ectopic (OFF), or both (ALL) dendrites of $A_{ON\text{-}S}$ RGCs compared with WT $A_{ON\text{-}S}$ RGCs. p value; **p < 0.01.

contrast, ~65% of $A_{ON\text{-}S}$ RGCs sampled in the DTA regions elaborated dendritic branches into the OFF layer (Figures 7A–7D). PSD95 puncta formed along $A_{ON\text{-}S}$ RGC dendrites in the OFF layer with a density similar to that of wild-type cells (Figure 7E). A substantial portion (78% ± 2%; n = 5 RGCs) of PSD95 puncta in the OFF layer were apposed to T2 BCs that are also Syt2-immunoreactive (Wässle et al., 2009) (Figure 7B), and the majority were apposed to ribbons (Figures 7C and 7F). Furthermore, cell-attached and whole-cell voltage-clamp recordings of $A_{ON\text{-}S}$ RGCs showed that cells with ectopic OFF dendrites had both ON and OFF light responses (n = 4), unlike $A_{ON\text{-}S}$ RGCs in wild-type mice from which only ON light responses could be evoked (n = 15) (Figures 7G-7L). The ON response amplitude was significantly less than normal (wild-type [WT]: 1503 ± 192 pA, n = 15; DTA: 635 ± 80 pA, n = 8; p < 0.01), most likely reflecting the loss of T6 BC connections and incomplete compensation by other ON-BC types. Selective blockade of ON-BC pathways with the mGluR6 agonist, L-2-amino-4-phosphonobutyric acid (L-AP4), abolished the ON response but spared the OFF response (n = 3), confirming that the OFF response was directly mediated by OFF-BCs (Figure 7L). The ectopic dendrites of $A_{ON\text{-}S}$ RGC thus selectively wired with T2 BCs, even though ON T5 and four other types of OFF BCs were still available.

DISCUSSION

Activity-driven competition for synaptic territory is a well-established developmental mechanism that shapes neuronal connectivity by synapse elimination. However, mechanisms must also be in place to regulate connectivity patterns of converging axons that retain contact with a postsynaptic cell. Here, we uncovered an unusual role of neurotransmission in regulating the number of synapses formed by an axon in a cell-autonomous, and thus noncompetitive, manner. Perhaps not unexpectedly, individual T6 axons that contact the $A_{ON\text{-}S}$ RGC make fewer synapses when they are transmission-suppressed, but surprisingly, their active neighbors do not increase their connectivity. Such cell-autonomous regulation occurred even though active and inactive axons formed synapses next to each other on the same dendrite, at distances that typically would allow alterations of synaptic drive from one input to affect connectivity of neighboring inputs (Engert and Bonhoeffer, 1997; Tao et al., 2001). Our finding thus contrasts with numerous examples in sensory systems where imbalanced activity among presynaptic cells differentially alters axonal size and synaptic territories of active and inactive cells

(F) Comparison of the percentage of PSD95 puncta that colocalized with CtBP2 in P21–P23 $A_{ON\text{-}S}$ RGCs. The bar graphs provide the mean + SEM. n, number of $A_{ON\text{-}S}$ RGCs. p values: **p < 0.01, ***p < 0.001.

(G–L) Light responses of a WT $A_{ON\text{-}S}$ RGC (G–I) and an $A_{ON\text{-}S}$ RGC with OFF dendrites in DTA-expressing region (J–L). Background light was maintained at the level of 700 photoisomerizations/rod/s (ON), and a dark spot (~360 µm diameter; 0 photoisomerization/rod/s) was applied over RGC's dendritic field for 1 s (OFF). Spike raster (G and J), spike rate (H and K), and excitatory postsynaptic current (I and L) are plotted. L-AP4 (10 µM).

See also Figure S2.

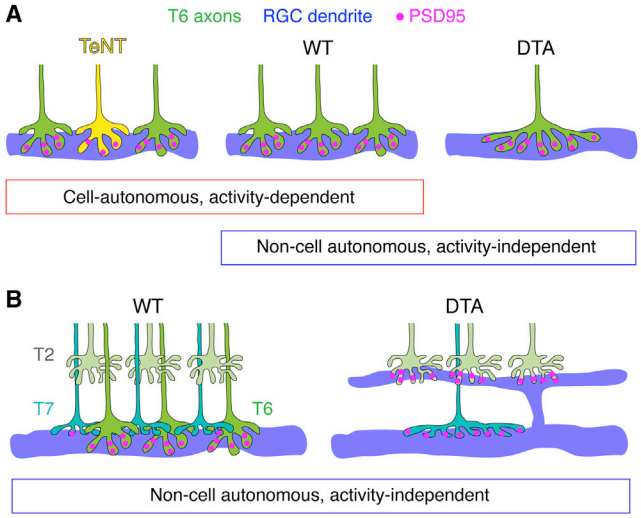

Figure 8. Summary of Developmental Processes that Determine the Number of Synapses Formed by Converging BC Axons onto a RGC

(A) With a single BC population, two mechanisms act together to regulate the synaptic connectivity of an individual axon. An activity-independent mechanism acts non-cell autonomously to restrict the number of synapses formed by T6 axons by constraining their axonal territories, whereas activity fine-tunes synapse numbers in a cell-autonomous manner without changes to axon size. (B) Presence, but not transmission, of the major input, T6 ON BCs, controls the connectivity of $A_{ON\text{-}S}$ RGCs with their minor input, T7 ON BCs. Presence of the major input also prevents dendritic mistargeting and synaptogenesis with T2 OFF BCs that are functionally mismatched with the $A_{ON\text{-}S}$ RGC.

(Antonini and Stryker, 1993; Yu et al., 2004; Hua et al., 2005; Ben Fredj et al., 2010).

Neighboring converging axons, however, do regulate connectivity of individual axons but through a non-activity-dependent mechanism possibly based on axon-axon interactions. Like their dendrites, the axonal arbors of the BCs tile. Tiling is adopted by many types of sensory neurons in invertebrates (Blackshaw et al., 1982; Grueber et al., 2002) and vertebrates (Sagasti et al., 2005; Wässle et al., 2009), and in its absence, neuronal arbors get altered in size and connectivity (Blackshaw et al., 1982; Sugimura et al., 2003; Emoto et al., 2004; Sagasti et al., 2005; Lee et al., 2011). Dendritic tiling clearly regulates the number of synapses impinging onto a neuron (Lee et al., 2011), but whether axonal tiling similarly regulates connectivity remained unresolved. We found that retinal BCs expand their axon territories in the absence of neighboring BCs and, in doing so, increase synaptic contact, a result not observed in our TeNT experiments. Thus, non-cell-autonomous regulation of BC axon territories and their connectivity is activity-independent. Because tiling preserves the orderly representation of visual space, this spatial constraint present during development may be advantageous; activity-mediated competition could produce unwanted variation in BC synaptic territories. But tiling by no means causes the circuit to be insensitive to changes in neuronal activity. Indeed, in mutants with abnormally high spontaneous BC activity, individual BC axons actually increase their connectivity (Soto et al., 2012); here, we show that individual axons with lowered activity decrease their synaptic contact. Whereas activity-independent mechanisms such as tiling place wiring limits on the circuit, transmission from axon terminals can fine-tune their individual connectivity without modification of the connections of their neighbors (Figure 8A). In other circuits sculpted by activity-dependent competition (Buffelli et al., 2003; Yu et al., 2004; Hua et al., 2005; Hashimoto et al., 2009a; Ben Fredj et al., 2010; Yasuda et al., 2011; Bleckert and Wong, 2011), neighboring axons generally overlap, which allows them to explore common space and compete for synaptic territory. BC axons in the retina may not evoke activity-dependent competition possibly because a tiling mechanism prevents such axonal overlap and exploration. Molecular factors mediating the tiling of BC axons are yet to be found. It will be interesting to test whether BC axons released from tiling constraints can recruit a synaptic competition mechanism driven by transmission (Bleckert and Wong, 2011).

Like many circuits in the nervous system, the laminar organization of axonal and dendritic arbors in the retina facilitates contact with appropriate synaptic partners (Yamagata et al., 2002; Yamagata and Sanes, 2008; Matsuoka et al., 2011a, 2011b). Our current observations, however, emphasize the role of lamination in dissuading synaptogenesis with incorrect partners. We found that $A_{ON\text{-}S}$ RGCs make ectopic connections with OFF BCs when ON T6 BCs are not available. Moreover, the ectopic dendrites of $A_{ON\text{-}S}$ RGC wired selectively with T2 BCs (Figure 8B), even though these dendrites coursed by the axonal fields of normally stratified ON T5 and four other types of OFF BCs. Dendritic targeting of a novel synaptic partner has been observed before, when the major input is missing, but in previous studies, the ectopic synapses are made with a limited set of available afferents nearby (Vrieseling and Arber, 2006; Haverkamp et al., 2006). Our current observations also indicate that misrouting of dendrites can occur despite the presence of molecular guidance cues, such as semaphorins, which appear to still be in place (Matsuoka et al., 2011a) in DTA-expressing retina because the remaining BCs were appropriately stratified. Thus, we uncovered an additional factor, an influence of the major input, in maintaining RGC dendrites within their correct sublamina. This dendritic maintenance is curiously activity-independent because blocking BC transmission does not result in misprojections of $A_{ON\text{-}S}$ RGC dendrites (Kerschensteiner et al., 2009). Thus, presence of presynaptic inputs, but not their activity, helps prevent the postsynaptic cell from connecting with other molecularly matched but functionally incompatible partners in the inner retina.

Finally, our ablation study unmasked another role of the major input in regulating the stereotypic patterns of synaptic convergence onto the RGC. In the absence of T6 BCs, $A_{ON\text{-}S}$ RGCs increase synaptic contact with T7 BCs, also an activity-independent process (Figure 8B). What factors could account for T6 BCs dominating synaptic connections onto $A_{ON\text{-}S}$ RGCs during normal development? One possibility is that contact with T6 BCs simply limit dendritic space available to T7 axons. This could occur if, compared to T7 BCs, T6 BCs differentiate earlier or form synapses before T7 BCs or, by virtue of their morphology, the axon terminals of T6 BCs overlap more with the stratified dendrites of $A_{ON\text{-}S}$ RGCs. Indeed, T7 BCs appear more strictly laminated compared to T6 BCs (Kerschensteiner

et al., 2009; Wässle et al., 2009; Helmstaedter et al., 2013). Another possibility is that T6 BCs actively suppress synapse formation with T7 BCs. For example, the interaction of $A_{ON\text{-}S}$ RGC dendrites with T6 BCs may trigger a signaling cascade within dendrites that dissuades contact with T7 BCs (Uemura et al., 2007) or axon-axon interactions may organize stereotypic synaptic innervation patterns of the two BC types sharing dendrites of the RGC. Indeed, axon-axon interactions have recently been demonstrated to carve out the synaptic territories of distinct types of motoneurons in *C. elegans* (Mizumoto and Shen, 2013). Finally, T6 and T7 BC axons may compete, without direct interactions, for a limited resource, but if so, this competition is not fueled by transmission because T7 BCs do not make more synapses when an overlapping T6 BC is inactive. Although the exact mechanisms that set up the dominance of an input have yet to be elucidated, our current observations together underscore a role for one input type in dictating connectivity of the postsynaptic cell by suppressing connections with other functionally compatible (ON) inputs as well as functionally incompatible (OFF) inputs via a transmission-independent process.

EXPERIMENTAL PROCEDURES

Transgenic Mice

We generated a construct comprising the sequence encoding YFP and a transcription stop signal, flanked by two LoxP sites, and the sequence for TeNT fused with CFP following the second LoxP site. This construct was placed downstream of a 9.5 kb fragment of the *Grm6* promoter (Ueda et al., 1997). *Grm6-TeNT* ^{patchy} and *Grm6-TeNT* ^{sparse} mice were derived from different founders during the process of generating transgenic mice driving expression of YFP and TeNT in retinal ON BCs under the control of the *Grm6* promoter. The screening process also identified a founder that expressed YFP and TeNT in all ON BCs (*Grm6-TeNT* ^{pan}). This line has also been used in previous studies (Kerschensteiner et al., 2009; Morgan et al., 2011). Variable expression patterns among different founders likely reflect differential regulation of the integrated transgene at different sites of the host genome. As previously described (Kerschensteiner et al., 2009), a very low level of TeNT-CFP was expressed and was sufficient to suppress neurotransmission without crossing with Cre driver lines. Thus, *Grm6-TeNT* mice were used without Cre-recombination. *Grm6-DTA* ^{con} mice were generated by replacing TeNT-CFP with a sequence encoding DTA (Tox176) (Breitman et al., 1990). A previous study had used the *Grm6-DTA* ^{con} mice without Cre-recombination and showed that BC density, $A_{ON\text{-}S}$ RGC morphology, and synapse density are unaltered in this line (Morgan et al., 2011).

Tissue Preparation

All experiments were conducted following animal protocols approved by the Institutional Animal Care and Use Committee at the University of Washington. All procedures in these protocols are in compliance with the National Institute of Health Guidelines for the Care and Use of Laboratory Animals. For immunohistochemistry and biolistic transfection, mice were euthanized with isoflurane followed by decapitation and enucleated. Each cornea was punctured with a 30G needle. The eyes were then transferred to oxygenated mouse artificial cerebrospinal fluid (mACSF) containing 119 mM NaCl, 2.5 mM KCl, 2.5 mM $CaCl_2$, 1.3 mM $MgCl_2$, 1 mM NaH_2PO_4, 11 mM glucose, and 20 mM HEPES at room temperature. mACSF was adjusted to pH 7.4 with 5 M NaOH. The cornea, lens, and vitreous were removed. For vibratome sections, the remaining eyecup was fixed for 13–20 min in 4% paraformaldehyde in mACSF, and the retina was isolated after fixation. For flat-mount preparations, the retina was isolated from the eyecup and mounted on a nitrocellulose membrane disc (Millipore) with retinal ganglion cell side up. The retinas were subsequently fixed for 20 min in 4% paraformaldehyde in mACSF. For electrophysiology, mice were dark adapted overnight and sacrificed by cervical dislocation under infrared illumination. Sections of retina were mounted photoreceptor side down on poly-lysine-coated cover slides (BD Biosciences) and perfused with oxygenated Ames solution (Sigma) heated at 32°C at a rate of 9 ml/min. After cell identification using dim light steps from darkness (0.5 photoisomerizations/rod/s), the retina was adapted to the background light intensity of 500–700 photoisomerizations/rod/s for at least 10 min prior to data collection.

Immunohistochemistry

For vibratome sections, retinas were embedded in 4% agarose (Sigma), sliced at 60 μm thickness, and incubated overnight at 4°C with primary antibodies. Thereafter, the slices were washed and incubated with secondary antibodies for 2 hr at room temperature. Flat-mounted retinas were incubated with primary antibodies for 5 days at 4°C, washed, and incubated with secondary antibodies overnight at 4°C. Vibratome sections and whole-mount retinas were mounted in Vectashield (Vector Laboratories). Primary antibodies used in this study were against Syt2 (znp-1; 1:1,000; mouse; Zebrafish International Resource Center), CaBP5 (1:400; rabbit; provided by Dr. F. Haeseleer), PKCα (1:1,000; mouse; Sigma), vGluT1 (1:1,000; guinea pig; Millipore), CtBP2 (1:1,000; mouse; BD Biosciences), red fluorescent protein (RFP) (1:1,000; rabbit; Clontech Laboratories), VAMP2 (1:1,000; mouse; Synaptic Systems), lucifer yellow (1:1,000; rabbit; Invitrogen), and SMI-32 (1:1,000; mouse; Covance). Secondary antibodies were anti-isotypic DyLight (1:1,000, Jackson ImmunoResearch) or Alexa conjugates (1:1,000, Invitrogen).

Biolistic Transfection

Gold particles (1.6 μm diameter; 12.5 mg; Bio-Rad) were coated with DNA plasmids encoding tdTomato (24 μg), PSD95-CFP (12 μg), or PSD95-mCherry (12 μg; gift from Dr. A.M. Craig) under the control of the cytomegalovirus promoter. The particles were delivered to retinal ganglion cells in whole-mount retinas using a Helios gene gun (40 psi; Bio-Rad). Transfected retinas were kept overnight in mACSF in a humid, oxygenated chamber at 33°C.

Image Acquisition

All the images were acquired with Olympus FV 1000 laser scanning confocal microscope. Images of whole-mount retinas were acquired using a 4× objective (numerical aperture [NA] 0.28) with a voxel size of 1.657 × 1.657 × 10 μm. All other images were acquired with a 60× oil objective (NA 1.35) at a voxel size of 0.103 × 0.103 × 0.3 μm or 0.082 × 0.082 × 0.25 μm.

Image Analysis

Acquired images were median-filtered using Fiji (Schneider et al., 2012). If necessary, image stacks were stitched to cover the entire retina using Fiji or to cover the entire dendritic arbor of $A_{ON\text{-}S}$ RGCs using Amira (Visage Imaging) and MATLAB (MathWorks). Dendrites of $A_{ON\text{-}S}$ RGCs were skeletonized using Imaris (Bitplane).

For mapping all the PSD95 puncta on the dendritic arbor of $A_{ON\text{-}S}$ RGCs, space surrounding the dendrites was masked to limit the search for potential puncta, and our custom-written, semiautomated program in MATLAB (Morgan et al., 2008) was used to locate all potential puncta. The identified potential puncta were projected onto the raw PSD95 image in 3D using Imaris. False positive and false negative selections were manually corrected. Our custom-written program identifies voxels belonging to each punctum, and we estimated the size of each punctum by multiplying the number of voxels of each punctum with voxel volume. Colocalization of PSD95 puncta with BC axons or CtBP2 puncta was assessed visually either in 3D using Imaris or Amira or plane-by-plane in 2D using a custom-written program in Matlab.

For analyzing pairs of BCs and $A_{ON\text{-}S}$ RGCs, axon terminals of BCs were segmented in 3D in Amira. The resulting mask was projected in 2D to estimate the axonal territory area, which was defined by the minimum convex polygon encompassing the mask. Axon-dendrite overlap was defined as the length of skeletonized dendrites that fell within the axonal territory area. Appositions and synapses with $A_{ON\text{-}S}$ RGCs were assessed visually in 3D using Amira.

To chart dendritic segments comprising largely active synapses or largely inactive synapses, we used a 12 μm sliding window to sample local short dendritic segments throughout the dendritic arbor (Figure 1F). If more than 85% of PSD95-CFP puncta within the window was apposed or not apposed to TeNT-expressing BCs, the dendritic segment was considered as inactive or active,

respectively. This window length was chosen because longer window lengths limited the total length of active or inactive dendritic segments available for analysis in each RGC. A shorter window length was not considered because the density of PSD95-CFP is on average only ~0.5 per μm (six puncta per 12 μm). Also, 12 μm approximates the diameter of an individual T6 BC axon terminal. Because rarely were all puncta "active" or "inactive" (100%) within a 12 μm length, we defined "active" and "inactive" segments as comprising at least 85% of puncta with the same identity.

After sampling all the active or inactive 12 μm dendritic segments, adjacent dendritic segments of the same type (either "active" or "inactive") were connected together. Although PSD95 puncta densities on individual RGCs in wild-type mice were relatively constant throughout the dendritic arbors (Morgan et al., 2008; Jakobs et al., 2008), proximal thick dendrites of $A_{ON\text{-}S}$ RGCs tended to have high PSD95 puncta density and distal dendrites tended to have lower PSD95 density, which could be due to insufficient time for trafficking PSD95-CFP to the most distal dendrites (Morgan et al., 2008). Thus, to compare PSD95 puncta density between active and inactive dendritic segments for each $A_{ON\text{-}S}$ RGC, dendrites whose distances from the center of the cell body were either less than 40 μm or more than 120 μm were disregarded. If the total number of active or inactive synapses did not exceed 25% of the sum of both synapse types, puncta density was plotted only for the dominant synapse type (Figure 1J). To examine PSD95 puncta density along the sharp transition between active and inactive dendritic segments in Figure 1K, pairs of neighboring active and inactive dendritic segments whose transitions occurred within 3 μm were sampled. Eighty-four such sharp transitions were found in 11 analyzed $A_{ON\text{-}S}$ RGCs. Each pair of neighboring active and inactive dendritic segments was centered (zero point on the x axis of Figure 1K) halfway of the transition to align the 84 dendritic segments for calculating the average PSD95 puncta densities.

Electrophysiology

$A_{ON\text{-}S}$ RGCs were targeted in retinal whole mounts based on somal size, and under cell-attached mode, the light responses were recorded. Cells with large somata and ON responses were then whole-cell voltage clamped as previously described (Murphy and Rieke, 2006; Schwartz et al., 2012). Excitatory synaptic current was measured at the reversal potential for inhibition (~−60 mV) experimentally determined for each recording. Visual stimuli were rendered on an organic light-emitting diode monitor (eMagin) and focused onto the photoreceptors through the microscope condenser. Dark circles (~360 μm diameter; −100% contrast) were centered on the receptive field of the target RGC and presented on a background light intensity of 500–700 photoisomerizations/rod/s. L-AP4 (Tocris) was applied in the perfusion at a concentration of 10 μM and washed in for at least 2 min prior to data collection. Peak excitatory postsynaptic current (EPSC) amplitudes for each cell were calculated based on mean traces derived from 5 to 20 repeats of the light stimulus. The mean traces were low pass filtered at 20 Hz to remove high-frequency synaptic noise, and peak ON and OFF EPSCs were measured in windows of 250 ms following the onset and offset of the light stimulus, respectively.

Statistics

Wilcoxon-Mann-Whitney rank-sum test was used for assessing statistical significance.

SUPPLEMENTAL INFORMATION

Supplemental Information includes three figures and one movie and can be found with this article online at http://dx.doi.org/10.1016/j.neuron.2014.02.016.

AUTHOR CONTRIBUTIONS

H.O., L.D.S., and R.O.L.W. conceived the experiments. H.O. and L.D.S. conducted imaging experiments. H.O. analyzed the images. G.W.S. performed and analyzed patch-clamp recordings. H.O., L.D.S., G.W.S., F.R., and R.O.L.W. wrote the paper.

ACKNOWLEDGMENTS

We thank Daniel Kerschensteiner and Renate Lewis for generating and screening transgenic mice used in this study, Mrinalini Hoon for proofreading the manuscript, and members of the Wong lab and Yukiko Goda for helpful discussions. This work was supported by the National Institute of Health (EY017101 to R.O.L.W., EY11850 to F.R., and the Vision Core Grant EY01730), the Howard Hughes Medical Institute (to F.R.), a Human Frontiers Science Program grant (to L. Lagnado, F. Schmitz, and R.O.L.W), and the Helen Hay Whitney Foundation (to G.W.S.).

Accepted: February 3, 2014
Published: April 2, 2014

REFERENCES

Antonini, A., and Stryker, M.P. (1993). Rapid remodeling of axonal arbors in the visual cortex. Science *260*, 1819–1821.

Ben Fredj, N., Hammond, S., Otsuna, H., Chien, C.B., Burrone, J., and Meyer, M.P. (2010). Synaptic activity and activity-dependent competition regulates axon arbor maturation, growth arrest, and territory in the retinotectal projection. J. Neurosci. *30*, 10939–10951.

Blackshaw, S.E., Nicholls, J.G., and Parnas, I. (1982). Expanded receptive fields of cutaneous mechanoreceptor cells after single neurone deletion in leech central nervous system. J. Physiol. *326*, 261–268.

Bleckert, A., and Wong, R.O. (2011). Identifying roles for neurotransmission in circuit assembly: insights gained from multiple model systems and experimental approaches. Bioessays *33*, 61–72.

Bleckert, A., Schwartz, G.W., Turner, M.H., Rieke, F., and Wong, R.O. (2014). Visual space is represented by nonmatching topographies of distinct mouse retinal ganglion cell types. Curr. Biol. *24*, 310–315.

Breitman, M.L., Rombola, H., Maxwell, I.H., Klintworth, G.K., and Bernstein, A. (1990). Genetic ablation in transgenic mice with an attenuated diphtheria toxin A gene. Mol. Cell. Biol. *10*, 474–479.

Buffelli, M., Burgess, R.W., Feng, G., Lobe, C.G., Lichtman, J.W., and Sanes, J.R. (2003). Genetic evidence that relative synaptic efficacy biases the outcome of synaptic competition. Nature *424*, 430–434.

Burrone, J., O'Byrne, M., and Murthy, V.N. (2002). Multiple forms of synaptic plasticity triggered by selective suppression of activity in individual neurons. Nature *420*, 414–418.

Cramer, K.S., Bermingham-McDonogh, O., Krull, C.E., and Rubel, E.W. (2004). EphA4 signaling promotes axon segregation in the developing auditory system. Dev. Biol. *269*, 26–35.

Davis, G.W. (2006). Homeostatic control of neural activity: from phenomenology to molecular design. Annu. Rev. Neurosci. *29*, 307–323.

DeNardo, L.A., de Wit, J., Otto-Hitt, S., and Ghosh, A. (2012). NGL-2 regulates input-specific synapse development in CA1 pyramidal neurons. Neuron *76*, 762–775.

Ding, J.B., Oh, W.J., Sabatini, B.L., and Gu, C. (2012). Semaphorin 3E-Plexin-D1 signaling controls pathway-specific synapse formation in the striatum. Nat. Neurosci. *15*, 215–223.

Emoto, K., He, Y., Ye, B., Grueber, W.B., Adler, P.N., Jan, L.Y., and Jan, Y.N. (2004). Control of dendritic branching and tiling by the Tricornered-kinase/Furry signaling pathway in Drosophila sensory neurons. Cell *119*, 245–256.

Engert, F., and Bonhoeffer, T. (1997). Synapse specificity of long-term potentiation breaks down at short distances. Nature *388*, 279–284.

Grueber, W.B., Jan, L.Y., and Jan, Y.N. (2002). Tiling of the Drosophila epidermis by multidendritic sensory neurons. Development *129*, 2867–2878.

Harms, K.J., Tovar, K.R., and Craig, A.M. (2005). Synapse-specific regulation of AMPA receptor subunit composition by activity. J. Neurosci. *25*, 6379–6388.

Hashimoto, K., Ichikawa, R., Kitamura, K., Watanabe, M., and Kano, M. (2009a). Translocation of a "winner" climbing fiber to the Purkinje cell dendrite

and subsequent elimination of "losers" from the soma in developing cerebellum. Neuron *63*, 106–118.

Hashimoto, K., Yoshida, T., Sakimura, K., Mishina, M., Watanabe, M., and Kano, M. (2009b). Influence of parallel fiber-Purkinje cell synapse formation on postnatal development of climbing fiber-Purkinje cell synapses in the cerebellum. Neuroscience *162*, 601–611.

Haverkamp, S., Michalakis, S., Claes, E., Seeliger, M.W., Humphries, P., Biel, M., and Feigenspan, A. (2006). Synaptic plasticity in CNGA3(-/-) mice: cone bipolar cells react on the missing cone input and form ectopic synapses with rods. J. Neurosci. *26*, 5248–5255.

Helmstaedter, M., Briggman, K.L., Turaga, S.C., Jain, V., Seung, H.S., and Denk, W. (2013). Connectomic reconstruction of the inner plexiform layer in the mouse retina. Nature *500*, 168–174.

Hua, J.Y., Smear, M.C., Baier, H., and Smith, S.J. (2005). Regulation of axon growth in vivo by activity-based competition. Nature *434*, 1022–1026.

Huang, L., Max, M., Margolskee, R.F., Su, H., Masland, R.H., and Euler, T. (2003). G protein subunit G gamma 13 is coexpressed with G alpha o, G beta 3, and G beta 4 in retinal ON bipolar cells. J. Comp. Neurol. *455*, 1–10.

Isope, P., and Barbour, B. (2002). Properties of unitary granule cell—>Purkinje cell synapses in adult rat cerebellar slices. J. Neurosci. *22*, 9668–9678.

Jakobs, T.C., Koizumi, A., and Masland, R.H. (2008). The spatial distribution of glutamatergic inputs to dendrites of retinal ganglion cells. J. Comp. Neurol. *510*, 221–236.

Kerschensteiner, D., Morgan, J.L., Parker, E.D., Lewis, R.M., and Wong, R.O. (2009). Neurotransmission selectively regulates synapse formation in parallel circuits in vivo. Nature *460*, 1016–1020.

Lee, S.C., Cowgill, E.J., Al-Nabulsi, A., Quinn, E.J., Evans, S.M., and Reese, B.E. (2011). Homotypic regulation of neuronal morphology and connectivity in the mouse retina. J. Neurosci. *31*, 14126–14133.

Marquardt, T., Ashery-Padan, R., Andrejewski, N., Scardigli, R., Guillemot, F., and Gruss, P. (2001). Pax6 is required for the multipotent state of retinal progenitor cells. Cell *105*, 43–55.

Masland, R.H. (2012). The neuronal organization of the retina. Neuron *76*, 266–280.

Matsuoka, R.L., Chivatakarn, O., Badea, T.C., Samuels, I.S., Cahill, H., Katayama, K., Kumar, S.R., Suto, F., Chédotal, A., Peachey, N.S., et al. (2011a). Class 5 transmembrane semaphorins control selective Mammalian retinal lamination and function. Neuron *71*, 460–473.

Matsuoka, R.L., Nguyen-Ba-Charvet, K.T., Parray, A., Badea, T.C., Chédotal, A., and Kolodkin, A.L. (2011b). Transmembrane semaphorin signalling controls laminar stratification in the mammalian retina. Nature *470*, 259–263.

Mizumoto, K., and Shen, K. (2013). Interaxonal interaction defines tiled presynaptic innervation in C. elegans. Neuron *77*, 655–666.

Morgan, J.L., Dhingra, A., Vardi, N., and Wong, R.O. (2006). Axons and dendrites originate from neuroepithelial-like processes of retinal bipolar cells. Nat. Neurosci. *9*, 85–92.

Morgan, J.L., Schubert, T., and Wong, R.O. (2008). Developmental patterning of glutamatergic synapses onto retinal ganglion cells. Neural Dev. *3*, 8.

Morgan, J.L., Soto, F., Wong, R.O., and Kerschensteiner, D. (2011). Development of cell type-specific connectivity patterns of converging excitatory axons in the retina. Neuron *71*, 1014–1021.

Murphy, G.J., and Rieke, F. (2006). Network variability limits stimulus-evoked spike timing precision in retinal ganglion cells. Neuron *52*, 511–524.

Napper, R.M., and Harvey, R.J. (1988). Number of parallel fiber synapses on an individual Purkinje cell in the cerebellum of the rat. J. Comp. Neurol. *274*, 168–177.

Palay, S.L., and Chan-Palay, V. (1974). Cerebellar Cortex: Cytology and Organization. (Berlin: Springer).

Phillips, M.A., Colonnese, M.T., Goldberg, J., Lewis, L.D., Brown, E.N., and Constantine-Paton, M. (2011). A synaptic strategy for consolidation of convergent visuotopic maps. Neuron *71*, 710–724.

Sagasti, A., Guido, M.R., Raible, D.W., and Schier, A.F. (2005). Repulsive interactions shape the morphologies and functional arrangement of zebrafish peripheral sensory arbors. Curr. Biol. *15*, 804–814.

Sanes, J.R., and Yamagata, M. (2009). Many paths to synaptic specificity. Annu. Rev. Cell Dev. Biol. *25*, 161–195.

Schneider, C.A., Rasband, W.S., and Eliceiri, K.W. (2012). NIH Image to ImageJ: 25 years of image analysis. Nat. Methods *9*, 671–675.

Schwartz, G.W., Okawa, H., Dunn, F.A., Morgan, J.L., Kerschensteiner, D., Wong, R.O., and Rieke, F. (2012). The spatial structure of a nonlinear receptive field. Nat. Neurosci. *15*, 1572–1580.

Shen, K., and Scheiffele, P. (2010). Genetics and cell biology of building specific synaptic connectivity. Annu. Rev. Neurosci. *33*, 473–507.

Soto, F., Ma, X., Cecil, J.L., Vo, B.Q., Culican, S.M., and Kerschensteiner, D. (2012). Spontaneous activity promotes synapse formation in a cell-type-dependent manner in the developing retina. J. Neurosci. *32*, 5426–5439.

Sugimura, K., Yamamoto, M., Niwa, R., Satoh, D., Goto, S., Taniguchi, M., Hayashi, S., and Uemura, T. (2003). Distinct developmental modes and lesion-induced reactions of dendrites of two classes of Drosophila sensory neurons. J. Neurosci. *23*, 3752–3760.

Tao, H.W., Zhang, L.I., Engert, F., and Poo, M. (2001). Emergence of input specificity of ltp during development of retinotectal connections in vivo. Neuron *31*, 569–580.

Turrigiano, G.G., and Nelson, S.B. (2004). Homeostatic plasticity in the developing nervous system. Nat. Rev. Neurosci. *5*, 97–107.

Ueda, Y., Iwakabe, H., Masu, M., Suzuki, M., and Nakanishi, S. (1997). The mGluR6 5′ upstream transgene sequence directs a cell-specific and developmentally regulated expression in retinal rod and ON-type cone bipolar cells. J. Neurosci. *17*, 3014–3023.

Uemura, T., Kakizawa, S., Yamasaki, M., Sakimura, K., Watanabe, M., Iino, M., and Mishina, M. (2007). Regulation of long-term depression and climbing fiber territory by glutamate receptor delta2 at parallel fiber synapses through its C-terminal domain in cerebellar Purkinje cells. J. Neurosci. *27*, 12096–12108.

Vrieseling, E., and Arber, S. (2006). Target-induced transcriptional control of dendritic patterning and connectivity in motor neurons by the ETS gene Pea3. Cell *127*, 1439–1452.

Wadiche, J.I., and Jahr, C.E. (2001). Multivesicular release at climbing fiber-Purkinje cell synapses. Neuron *32*, 301–313.

Wässle, H., Puller, C., Müller, F., and Haverkamp, S. (2009). Cone contacts, mosaics, and territories of bipolar cells in the mouse retina. J. Neurosci. *29*, 106–117.

Williams, M.E., de Wit, J., and Ghosh, A. (2010). Molecular mechanisms of synaptic specificity in developing neural circuits. Neuron *68*, 9–18.

Yamagata, M., and Sanes, J.R. (2008). Dscam and Sidekick proteins direct lamina-specific synaptic connections in vertebrate retina. Nature *451*, 465–469.

Yamagata, M., Weiner, J.A., and Sanes, J.R. (2002). Sidekicks: synaptic adhesion molecules that promote lamina-specific connectivity in the retina. Cell *110*, 649–660.

Yasuda, M., Johnson-Venkatesh, E.M., Zhang, H., Parent, J.M., Sutton, M.A., and Umemori, H. (2011). Multiple forms of activity-dependent competition refine hippocampal circuits in vivo. Neuron *70*, 1128–1142.

Yu, C.R., Power, J., Barnea, G., O'Donnell, S., Brown, H.E., Osborne, J., Axel, R., and Gogos, J.A. (2004). Spontaneous neural activity is required for the establishment and maintenance of the olfactory sensory map. Neuron *42*, 553–566.